Bull. Mater. Sci., Vol. 28, No. 7, December 2005, pp. 675–679. © Indian Academy of Sciences.

Optical, thermal and phase transition studies in $Sn_{1-x}Ge_xTe$

M SIVABHARATHY[†], N SANKAR, R SARAVANAN and K RAMACHANDRAN*

School of Physics, Madurai Kamaraj University, Madurai 625 021, India
[†]Department of Physics, S.C.K. College, Tenkasi 627 804, India

MS received 15 June 2005

Abstract. The optical and thermal properties of the mixed semiconducting alloy, $Sn_{1-x}Ge_xTe$, is studied by photo acoustics, for various Ge concentrations and phase transition for a particular concentration is also studied by the same method. The results are compared with the available literature values and discussed.

Keywords. Optical properties; thermal properties; $Sn_{1-x}Ge_xTe$; phase transition.

1. Introduction

It is known that IV–VI compound semiconductors are used for infrared detectors (An and Banderia 1985). In such fabrications, a complete study on optical and thermal properties are very much essential. Similarly an idea of phase transition with temperature is necessary for such detectors. Mechanisms are available to monitor the thermal behaviour of solids, by DSC and the TG/DTA but these methods involve direct heating of the sample in a heat source. Also, the sample is destroyed and could not be retrieved for other measurements. But it has been well proved by Ganguly and Rao as early as in 1986 that DSC or TG/DTA studies cannot give the exact transition temperature when the material undergoes a phase transition and photoacoustics is the best tool for such studies. This we have demonstrated in our recent paper on *L*-alaninium oxalate (Sivabharathy *et al* 2004). The photoacoustic (PA) technique is one of the simplest and fastest technique that provides information not only on thermal parameters but also on the carrier transport properties (Chu *et al* 2001; Yoshida 2001) and useful in the study of phase transition (Sivabharathy *et al* 2004). Similarly optical absorption or UV–VIS study can be straightaway deduced from the photoacoustic measurements.

Ferreira *et al* (1989) have reported photoacoustic measurements on the thermal diffusivity of $Pb_{1-x}Sn_xTe$ where thermally thick samples are studied for various compositions. Eventhough the expected behaviour of the thermal diffusivity for the binary mixtures, PbTe and SnTe, is monotonic, the experiment shows that there are few maxima in the graph. Particularly between the concentrations 0·02 and 0·2, the variation in the thermal diffusivity is not monotonic whereas there are two maxima. For $Sn_{1-x}Ge_xTe$ such studies are not reported, even though electrical and optical studies are available (Nussbaum 1954; Rosenman 1963; Lanyon 1964; Beyer *et al* 1969; Sutter 1969; Kessler and Sutter 1971; Dawar *et al* 1981).

Germanium telluride (GeTe) is known to undergo phase transition from a cubic structure to a rhombohedrally distorted low temperature phase (Korzhuev 1982). The transition temperature lies between 625 and 690 K and it is found to be difficult to find out the exact value as the material started decomposing at those temperatures.

In the case of tin telluride (SnTe), a soft optic phonon appears in the neutron scattering below the room temperature (Cowley 1969). Elastic neutron scattering (Iizumi 1975) and X-ray diffraction by Muldawer (1973) indicate that the concentration of free charge carriers (holes) plays an important role in the structural phase transition in SnTe. The sample with hole concentration below $10^{20}/cm^3$ undergoes complete transformation. Iizumi *et al* (1975) reported a transition at 98 K with low carrier concentration.

SnTe, PbTe, PbS, $Pb_{1-x}Sn_xTe$, $Pb_{1-x}Ge_xTe$ and $Pb_{1-x}Ge_xS$ are some important and well studied IV–VI systems as far as the phonon properties, thermal properties and phase transition studies are concerned (Fano *et al* 1977). But such studies for $Sn_{1-x}Ge_xTe$ are very rarely seen in literature and photoacoustic study is not at all available.

In order to study these important optical, thermal and phase transition properties, photoacoustic study is carried out here for $Sn_{1-x}Ge_xTe$, particularly for very low concentrations of Ge, as any anamolous behaviour in thermal diffusivity can be easily seen in these concentrations as in $Pb_{1-x}Sn_xTe$.

2. Crystal growth and sample preparation

The crystals were grown by Bridgmann method. Conically tipped growth ampoules are made from silica tubes for

*Author for correspondence (thirumalchandran@yahoo.com)

growth. No dependence on crystal quality was observed on the cone angle variation from 30–45°. Before loading the starting materials, the ampoules are cleaned with detergent and hot water for removing dust and grease. Absorbed inorganic chemicals and adsorbed detergents are removed by washing with HNO_3 containing HF. Traces of acid are removed by aqua regia and distilled water. Finally the ampoules are heated in the furnace at 500°C for 1 h.

Appropriate weights of the elements were loaded into the ampoule, which was then evacuated (~ 10^6 Torr) and sealed. The charge was melted in a vertical furnace whose temperature was increased slowly and maintained at about a temperature of 100 K more than the melting point. The growth velocity and the temperature gradient for getting good single crystal are 0·2 mm per hour (moving from the hot zone to cold zone of the furnace) and 100 K per cm. In order to reduce the precipitation of free Te, proper care was taken with (Ge + Sn): Te as stoichiometric. To produce samples in the desired compositional range, melts containing about 20–40% GeTe were used. Single crystalline sections were selected from the tip regions of the boules, and cut into samples of about 2 × 3 × 1 mm size. Two faces were polished plane and parallel to the quality usually required for further measurements.

Preliminary X-ray studies are carried out to identify the samples. The lattice parameters, densities and the preliminary Bragg peaks suggest that the grown samples are $Sn_{1-x}Ge_xTe$.

3. Photoacoustic (PA) spectrometer

In photoacoustic spectroscopy (PAS), periodic heat emission produces varying pressure inside the cell where the sample placed in an air tight photoacoustic cell is exposed to intensity modulated light. This is detected as the photoacoustic signal. The schematic diagram of the present PA spectrometer is shown in figure 1. Model FL-1039, 450 W Xenon lamp housing with all reflective optics (Jobin Yvon Inc., USA) is used as the source. Model TR180FST1X (SPEX), Triax-180, f/3·9 imaging spectrometer including fixed entrance slit assembly, patented kinematic triple grating turret with on-axis grating rotation of model HS 1000, handscan-hand held controller is used as the monochromator. A light chopper, Model 651 (Perkin Elmer) that is a quartz crystal oscillator for the primary frequency standard is employed. Like many other choppers, the chopping frequency can be controlled externally. However, unlike other units the control is via an applied TTL reference pulse rather than analog voltage and so one can exactly obtain the required modulation frequency. The modulation frequency varies from 6–3200 Hz. Model 7225 DSP Lock-in Amplifier (Perkin Elmer), is used to recover the PA signal from the microphone.

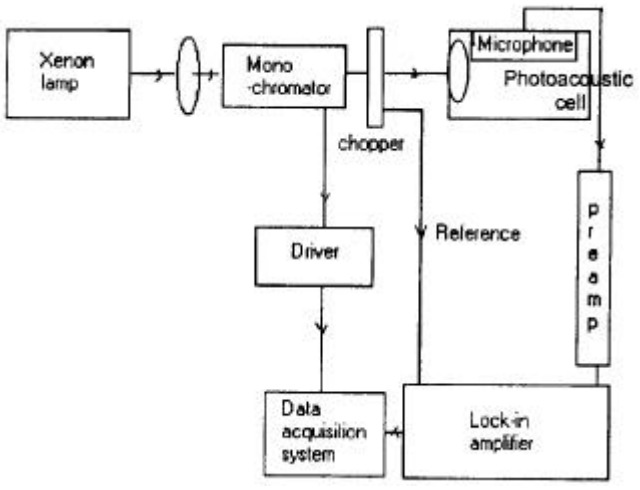

Figure 1. Schematic diagram of the PA set up.

The design of the PA cell is critical to ensure a very good signal to noise ratio. Theoretical and experimental studies predict that for a constant light absorption, the amplitude of the photo acoustic signal reaching the microphone depends on the size of the cell and in general increases as cell dimensions are reduced. However, one must not minimize this to a point, that the acoustic signal produced at the sample suffers appreciable dissipation to the cell window and walls, before reaching the microphone. Proper acoustic isolation from outside world and the microphone configuration are also critical. Most importantly the sample to be studied also plays a significant role in designing a photo acoustic cell. Taking these (constraints) into consideration, a variable temperature photo acoustic cell, enclosed within an airtight vacuum container made of stainless steel, is designed. The vacuum around the PA cell minimizes the external noise. The sample was mounted in the cell, over which a 32 gauge nichrome wire was wound for heating the PA cell, so that phase transition can be studied above room temperature. Below the heating element a thermocouple is attached for temperature measurements. The actual PA cell, which is used for the measurements, is shown in figure 2.

3.1 *Measurements*

For the optical and thermal properties, PA measurements are done in two ways: (i) first keeping wave length of the incident light constant, PA signal amplitude is recorded for various chopping frequencies (figure 3) for the different samples (called the depth profile analysis); and (ii) secondly keeping the modulation frequency constant, PA signals are recorded by varying the wavelength (figure 4) at room temperature (called the photoacoustic spectrum).

For thermal properties, the depth profile is enough and the photoacoustic spectrum is useful for optical studies.

For the thermally thin (l) samples, knowing the characteristic frequency, f_c, the thermal diffusivity is calculated using

$$a = f_c\, l^2\ \mathrm{cm^2\ s^{-1}}. \tag{1}$$

(Characteristic frequency is an unique parameter for any material. When a photon of energy, E, is incident on a sample, the thermal energy cannot diffuse into this material to infinite depth and it will reach only up to the thermal diffusion length, which is another unique parameter. The sample that is used for PA measurements should have thickness lower than the thermal diffusion length. This is a thermally thin sample. If it is the other way, this is known as a thermally thick sample. Characteristic frequency is the frequency at which sample goes from thermally thick to thermally thin region).

The thermal effusivity is

$$e = \sqrt{f_c l^2 r c_p^2}\ \ \mathrm{Ws^{1/2}/cm^2\ K}, \tag{2}$$

where r is the density, and c_p the specific heat capacity of the sample.

The thermal conductivity now is

$$K = a\ r\ c_p\ \mathrm{W/cm\ K}. \tag{3}$$

From figure 3, the characteristic frequencies are first found out for the different samples. Then the thermal parameters are worked out from (1) and (2).

Even though no such measurements are reported in the literature for these alloys, for comparison of our results, we computed the same from the values of the end members, SnTe and GeTe. This is done following the theory of binary mixtures as

$$a_{\mathrm{eff}} = \frac{(1-x)k_1 + xk_2}{(1-x)\,r_1c_1 + xr_2c_2}, \tag{4}$$

where the subscripts 1 and 2 refer to SnTe and GeTe, respectively, r and c denote density and specific heat. Using $r_1 = 6{\cdot}44$ g/cm^3, $c_1 = 0{\cdot}41$ J/gk, $k_1 = 0{\cdot}0692$ W/cm K, $r_2 = 6{\cdot}16$ g/cm^3, $c_2 = 0{\cdot}112$ J/gk and $k_2 = 0{\cdot}0687$ W/cm K, we have thus calculated a_{eff} and plotted in the same figure 5. A good agreement is seen. Similarly the measured thermal conductivity for various concentrations of Ge are given in table 1.

The results show that thermal diffusivity increases with increase in the concentration of Ge. The variation also shows that this alloy retains the crystalline form, as amorphous systems will generally show a positive slope.

Similarly from the photoacoustic spectrum (figure 4), we can estimate the optical band gap of these $Sn_{1-x}Ge_xTe$ samples. Since SnTe and GeTe are direct band gap materials, these are also expected to be direct band gap materials and the energy gap, E_g, is deduced from the equation

$$(b\ hn)^2 = C\ (E - E_g - E_{\mathrm{phonon}})^2, \tag{5}$$

where E is the incident photon energy, E_g the band gap and E_{phonon} the phonon emitted or absorbed during the indirect transition and C a constant. For direct band gap materials, there is no phonon involved in the transition and so E_{phonon} is zero.

The E_g values obtained from figure 4 and eqn. (5) are given in table 2. As done earlier, we have estimated the expected value of the band gap by using Vegard's law and the end member values, if there is no phase transition.

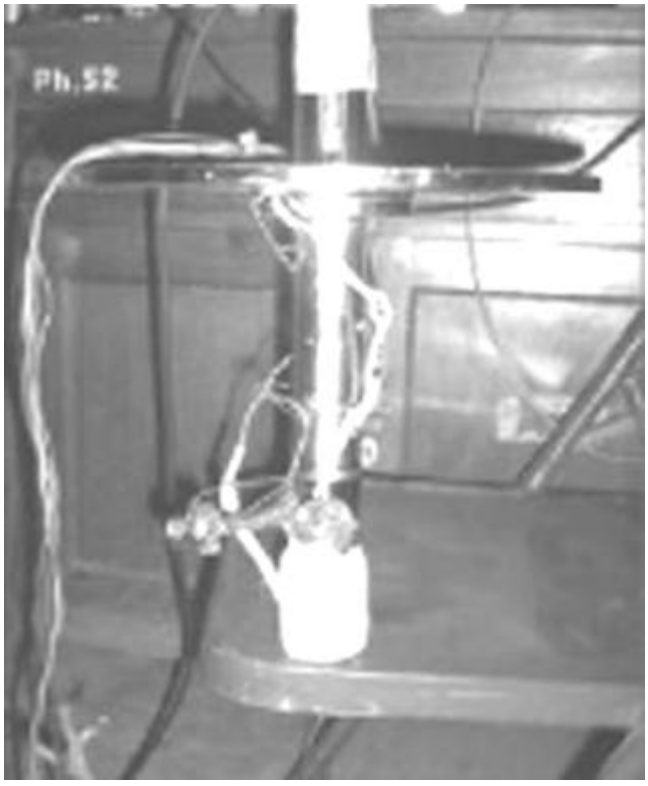

Figure 2. The actual PA cell used for PA measurements.

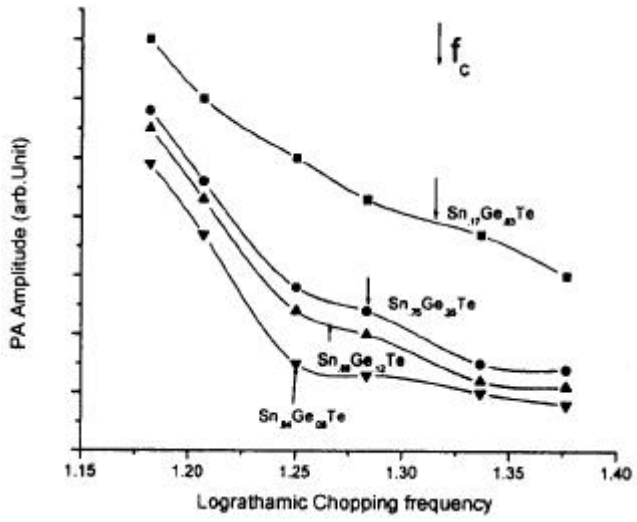

Figure 3. Variation of PA signal amplitude with chopping frequency.

Table 1. Measured and computed thermal diffusivity, a.

Sample	Thermal diffusivity, a (cm^2s^{-1})	Calculated a (cm^2s^{-1})	Thermal conductivity, K (W/cmK)
GeTe (Rosi 1960)	0·997	–	0·0687
$Sn_{0·17}Ge_{0·83}Te$	0·770	0·767	0·0663
$Sn_{0·75}Ge_{0·25}Te$	0·181	0·186	0·0683
$Sn_{0·88}Ge_{0·12}Te$	0·161	0·165	0·0687
$Sn_{0·94}Ge_{0·06}Te$	0·117	0·118	0·0689
SnTe (Ferreira *et al* 1989)	0·026	–	0·0692

No other measurements are reported for energy gap for these concentrations and so we compared only with the Vegard's values. For low concentrations of Ge, the agreement is good. For other concentrations, one has to carry out some more verifications whether any phase transitions are present with respect to concentrations.

4. PA measurements on phase transition due to temperature

In this §, we carry out measurements for only one sample, $Sn_{0·17}Ge_{0·83}Te$, as we intend to demonstrate that PA is one of the best tools available for phase transition compared to the others mentioned in the earlier §. Moreover, this sample after the experiment can still be used for further experiments and above all the sample that we choose has a very convenient transition temperature of about 400 K, expected from the end members which is well above the room temperature. So, low temperature measurements are not required.

The sample, $Sn_{0·17}Ge_{0·83}Te$, was heated from ambient to 500 K with a heating rate of 1°C/min. A commercial electrically heated tubular furnace was used for this purpose connected to a PID temperature control.

The measured PA signal for different temperatures is shown in figure 6. At 446 K, there is an abrupt fall in the amplitude of the PA signal for this $Sn_{0·17}Ge_{0·83}Te$ sample.

Common to all measured PA signals against temperature is the negative temperature coefficient far away from the transition point. About 10 K above T_c, PA signals start to decrease and continue to do so at an increasing rate until the transformation temperature is reached. This is very much seen in figure 6.

In order to confirm this transition at 446 K, the experiment is repeated for the cooling cycle also i.e. when the temperature is reduced at a rate of 1°C/min down to room temperature, PA signal is again observed for each temperature. Here the transition is observed at 440 K.

So, the sample, $Sn_{0·17}Ge_{0·83}Te$, is identified to have a phase transition at 440 K. From Vegard's law, the transition temperature is 446 K. The agreement is very good and it is again proved that the present PA method is very effective in determining the phase transition.

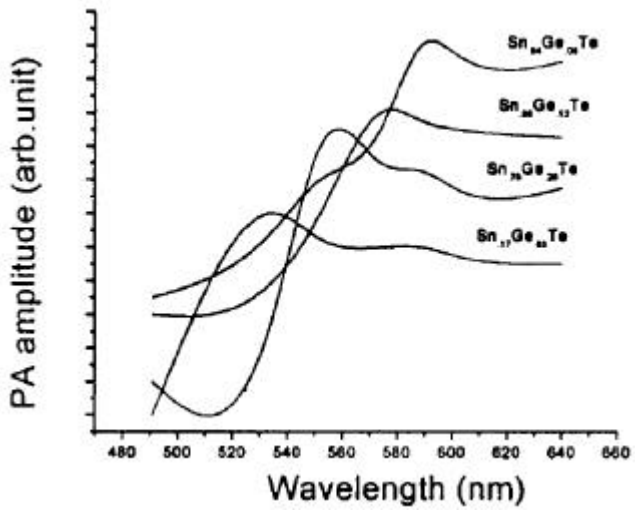

Figure 4. Variation of PA signal amplitude with wavelength for a chopping frequency of 25 Hz.

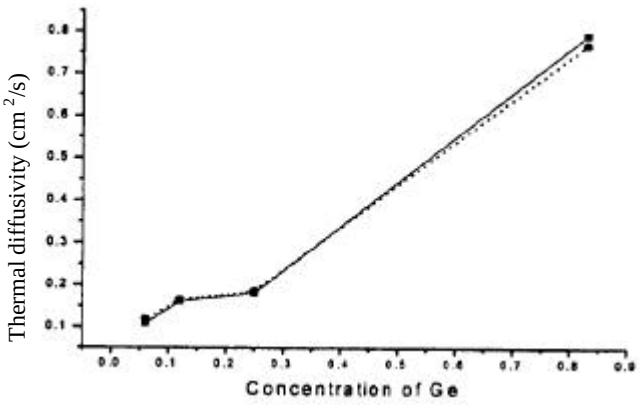

Figure 5. Variation of thermal diffusivity with concentration of Ge. (Solid line, measured diffusivity; points, expected values).

5. Discussion

SnTe in paraelectric phase itself has some interesting behaviour. The measured phonon dispersion in [100] showed a kink near the zone centre which is an unusual behaviour as far as any system is concerned (Brillson and

Table 2. Energy gap measured from PA spectrum (figure 4).

Sample	Energy gap (eV)	Energy gap (eV) expected (Vegard law)
GeTe (Korzhuev 1982)	–	0·93
$Sn_{0.17}Ge_{0.83}Te$	0·7	0·80
$Sn_{0.75}Ge_{0.25}Te$	0·3	0·37
$Sn_{0.88}Ge_{0.12}Te$	0·25	0·27
$Sn_{0.94}Ge_{0.06}Te$	0·2	0·225
SnTe (Ferreira *et al* 1989)	–	0·18

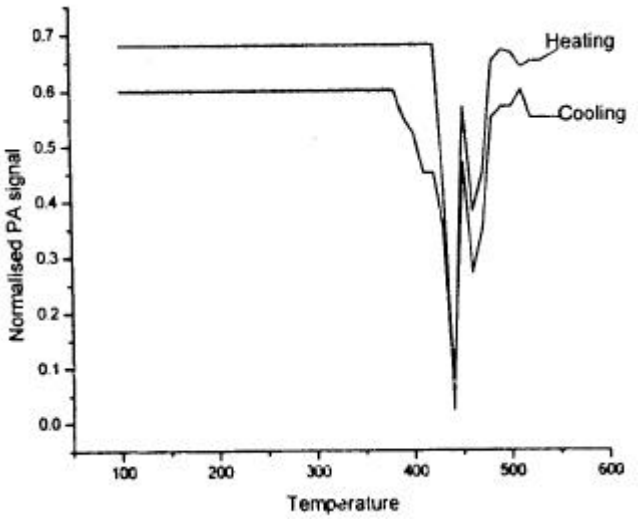

Figure 6. The variation of PA signal with temperature.

Burstein 1974). This was investigated lattice dynamically (Ramachandran and Haridasan 1979) and showed that the dielectric screening is dominant in this system. So, a mixed system like $Sn_{0.17}Ge_{0.83}Te$ is also expected to have some unusual behaviours as far as the thermal properties are concerned, as they are essentially due to phonons. Now in the present PA measurements for the SnTe rich, $Sn_{1-x}Ge_xTe$, we could see this effect as in figure 5, where for Ge = 0·12, there is a kink compared to the other concentrations. Incidentally this is what it has been reported for $Pb_{1-x}Sn_xTe$ (Ferreira *et al* 1989). Ferreira *et al* (1989) studied thermal diffusivity and thermal conductivity by PA technique for $Pb_{1-x}Sn_xTe$ as a function of the concentration, *x*, where atleast two to three kinks are observed. To understand this they have computed the electronic contribution to the thermal conductivity and concluded that this kink is exclusively due to lattice thermal diffusivity. This is what we predict from the behaviour of the phonons or otherwise the lattice property as the PA experiment is basically heat diffusion and acoustic wave generation.

6. Conclusions

$Sn_{1-x}Ge_xTe$ samples are synthesized first for various concentrations, by Bridgmann technique and preliminary characterizations were done to identify the grown samples and the concentrations. Photoacoustic measurements are made on these $Sn_{1-x}Ge_xTe$ samples, particularly in the Sn rich regime. Optical and thermal properties are measured from the PA spectra which compare well with interpolated values. Similarly, the same experiment is used to study the phase transition, particularly for a sample where the transition temperature is expected to be above room temperature. Again it compares with the interpolated values of the end members.

This is the first ever experimental report for this alloy simultaneously for the optical, thermal properties and phase transition.

References

An C Y and Banderia I N 1985 *Brazilian Rev. Appl. Phys. Instrum*. **1** 52

Beyer W, Mell H and Stuke J 1969 *Phys. Status Solidi* **33** 749

Brillson L J and Burstein E 1974 *Phys. Rev.* **B9** 1547

Cowley E R, Darby J K and Pawley G S 1969 *J. Phys. C (Solid State Phys.)* SER 2, **2** 1916

Chu Dachen, Touzelbaev Maxat, Goodson Kenneth E, Babin Sergey and Fabian Pease R 2001 *J. Vac. Sci. Technol.* **B19** 2874

Dawar A L, Joshi J C and Narain C 1981 *Thin Solid Films* **76** 113

Fano V, Fedeli G and Ortali I 1977 *Solid State Commun.* **22** 467

Ferreira S O, Ying An C, Bandeira I N and Miranda L C M 1989 *Phys. Rev.* **B39** 7967

Iizumi M, Hamaguchi Y, Komatsubara K F and Kato Y 1975 *J. Phys. Soc. Jap.* **38** 443

Kessler R and Sutter E 1971 *Phys. Status Solidi* **(b)45** 153

Korzhuev M A 1982 *Phys. Status Solidi* **(b)112** K39

Lanyon H P D 1964 *J. Appl. Phys.* **35** 1516

Muldawer L 1973 *J. Nonmetals* **1** 117

Nussbaum A 1954 *Phys. Rev.* **94** 337

Ramachandran K and Haridasan T M 1979 *Indian J. Phys.* **A53** 97

Rosenman L 1963 *Phys. Status Solidi* **3** 1429

Rosi F D, Dismukes J P and Hockings E F 1960 *Elec. Eng.* **79** 450

Sivabharathy M, Natarajan S, Ramakrishnan S K and Ramachandran K 2004 *Bull. Mater. Sci.* **27** 403

Sutter E 1969 *Phys. Status Solidi* **33** 749

Yoshida Atsumasa, Nogami Hideo, Kurita Takashiro and Washio Selichi 2001 *Anal. Sci.* **17** 154